Catalysis Science & Technology

Accepted Manuscript

ROYAL SOCIETY OF CHEMISTRY

www.rsc.org/catalysis

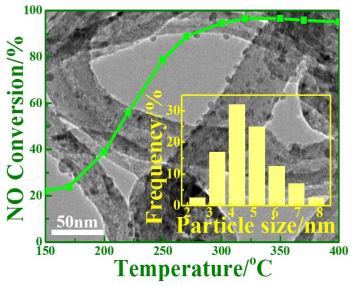

The Fe_2O_3 nanoparticles *in situ* anchored on carbon nanotubes via an ethanol-thermal strategy present an excellent $DeNO_x$ performance.

Journal Name

RSCPublishing

ARTICLE

Fe_2O_3 Nanoparticles *in situ* Anchored on Carbon Nanotubes via an Ethanol-thermal Strategy for Selective Catalytic Reduction of NO with NH_3

Jin Han, Dengsong Zhang*, Phornphimon Maitarad, Liyi Shi, Sixiang Cai, Hongrui Li, Lei Huang, Jianping Zhang

Cite this: DOI: 10.1039/xoxxoooooox

Received ooth January 2012,
Accepted ooth January 2012

DOI: 10.1039/xoxxoooooox

www.rsc.org/

Fe_2O_3 nanoparticles were *in situ* anchored on carbon nanotubes (CNTs) via an ethanol-thermal route for selective catalytic reduction (SCR) of NO with NH_3. The structure and surface characteristics of the obtained catalysts were measured by transmission electron microscope, X-ray diffraction, N_2 adsorption-desorption isotherms, Raman, X-ray photoelectron spectroscopy, H_2-temperature programmed reduction, and NH_3-temperature programmed desorption. Compared with the catalysts prepared via impregnation or co-precipitation methods, the synthesized catalyst showed the better catalytic activity and the more extensive operating-temperature window. The TEM and XRD results suggested that the iron species was uniformly anchored on the surface of CNTs. The Raman and XPS results indicated that the catalyst has a relatively higher defects and atomic concentration of Fe existed on the surface of CNTs and the higher content of chemisorbed oxygen species. The H_2-TPR and NH_3-TPD results demonstrated that the catalyst possessed the more powerful reducibility and stronger acid strength than the other two catalysts. Based on the above mentioned physicochemical properties, the obtained catalysts showed an excellent performance in the SCR of NO to N_2 with NH_3. Besides, the catalysts also presented outstanding stability, H_2O resistance and SO_2 tolerance.

1. Introduction

Nitrogen oxides (NO_x), which comes from the combustion of fossil fuels in the industrial, can result in some environmental contamination, such as acid rain, photochemical smog and air haze.[1-4] Nowadays, a certain of processes have been employed to remission these environmental problems.[4-10] Among these methods, the selective catalytic reduction (SCR) technology has been one of the state-of-the-art processes through the reductant-NH_3 selective chemical reaction with NO_x to form the environmental products N_2 and H_2O.[5, 6] The commercial catalysts, V_2O_5-WO_3 (MoO_3) /TiO_2, have been widely used for NO_x elimination.[4-6] However, there still remains some inevitable problems unsolved, such as low N_2 selectivity while at high temperature, the volatility and toxicity of V_2O_5.[5, 11-13] What's more, the notable oxidation of SO_2 to SO_3 could cause the etching of the equipment and blocking the pores of the catalysts.[5, 11, 12] So it is meaningful to design and develop a suitable non-vanadium catalyst with a relative low working temperature and a great resistance of SO_2 toxicity.[11, 14, 15]

Iron, as an ordinary element of the transition-metal block, has been widely investigated either as an active ingredient or promoter for $DeNO_x$ catalysts according to its inherently environmentally character, the prominent thermal stability and the outstanding performance of SO_2 resistance, such as Fe_2O_3,[16] Fe/ZSM-5,[11, 17-22] Fe/HBEA,[23, 24] Au/Fe_2O_3,[25] Fe_2O_3-TiO_2,[26] and Fe_2O_3-CeO_2/TiO_2.[27] Catalytic performance and mechanism of Fe zeolites in the NH_3-SCR have been studied systematically,[11, 17-24] as well as the ferric oxides applied as additive agent.[13, 14, 27] However, as the NH_3-SCR of NO applications are always in downstream after the desulfurizer and electrostatic precipitator, so it is still necessary to improve the low temperature activity of ferric oxides catalysts.

Recently, carbon nanotubes (CNTs) were demonstrated to possess the outstanding features of adsorption of ammonia, nitric oxides and other gaseous substances.[28-31] Besides, CNTs could decompose and directly reduce NO,[32, 33] and improve the SO_2 resistance with downing the decomposition temperature of sulfates and bisulfates.[34, 35] Hence, CNTs have attracted great attention towards NH_3-SCR of NO.[36-39] It is considered that the good dispersion of active ingredients on the support could be in favor of the activity during the NH_3-SCR reaction,[40, 41] and thus it is significant to realize the active species with smaller size highly dispersed on the support. Normally, the CNTs-carried

catalysts were synthesized by an impregnation method[36, 42] or sol-gel method.[26, 35, 43, 44] However, the active nanoparticles couldn't be uniformly dispersed on the surface of the CNTs by using these routes. Therefore, there still remains a great challenge to uniformly disperse the active species on the CNTs. Recently, we *in situ* accomplished MnO_x-CeO_x nanoparticles supported on CNTs via a surfactant assisted reflux route[41] and pyridine-thermal route,[45] and found that they all displayed enhanced NH_3-SCR activity and improved resistance of SO_2 and H_2O than the same catalyst synthesized by an impregnation method.

Herein, we rationally designed and originally prepared highly dispersed Fe_2O_3 nanoparticles on CNTs. As illustrated in Scheme 1, Fe_2O_3 nanoparticles were *in situ* anchored on CNTs by an ethanol-thermal strategy. Firstly, the Fe^{3+} interacts with the hydroxyl and carboxyl groups on the surface of the pretreated CNTs due to the electrostatic effect. Secondly, the ethonal might bond with the Fe^{3+} through the strongly electronegative end to finish the Fe^{3+} electric neutrality. After the solvothermal process and calcination, the Fe_2O_3 nanoparticles were *in situ* anchored on the CNTs. In this synthetic process, the steric hindrance of ethanol can effectively separate each of the Fe^{3+}, and thus highly dispersed Fe_2O_3 nanoparticles were *in situ* formed on CNTs. The obtained catalysts were characterized systematically, and their NH_3-SCR activity, stability, H_2O resistance and SO_2 tolerance were also investigated.

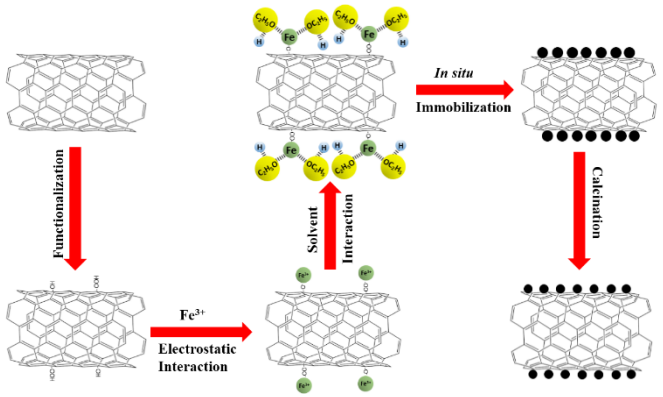

Scheme 1 Schematic illustration of the *in situ* synthetic process of the Fe_2O_3/CNTs-ET catalyst.

2. Experimental

2.1 Catalyst preparation

The multiwall carbon nanotubes (CNTs) were furnished by Qinhuangdao Tai Chi Ring nano products Co. Ltd (China). All the other chemicals were purchased from Sinopharm Chemical Regent Company and used without any further purification. The raw CNTs were 1-10 μm in length and 10-30 nm in diameter. The CNTs were pretreated with refluxed in dilute HNO_3 (6 mol/L) under stirring for 6 h at 120 °C to remove metal species and impurities that existed in the surface of raw CNTs; and then washed with abundance deionized water till pH neutral, and dried at 100 °C in oven overnight.

In a typical synthesis, 0.23 g of pretreated CNTs, 0.03 g of iron (III) nitrate nonahydrate and 80 mL of ethanol were mixed with the subsequent ultrasonic treatment at room temperature for 0.5 h. Then the mixture was poured into a stainless steel autoclave with PTFE lining (100 mL) and maintained at 120 °C for 24 h. After the autoclave was cooled to ambient temperature, the suspension was filtered and washed, and then dried at 100 °C for 12 h. Finally, it was calcined in N_2 stream at 450 °C for 4 h with the heating rate of 2 °C/min. The obtained catalyst was denoted as Fe_2O_3/CNTs-ET.

For comparison, the catalysts were also prepared by impregnation and co-precipitation methods, respectively. In the impregnation procedure, 0.69 g of pretreated CNTs were added in the solution of iron (III) nitrate nonahydrate (0.09 g) and H_2O (80 mL) with stirring till the solution dried at 80 °C, and then calcined in N_2 stream at 450 °C for 4 h with the heating rate of 2 °C/min. The catalyst synthesized by this method was denoted as Fe_2O_3/CNTs-IM. In the co-precipitation procedure, 0.23 g of pretreated CNTs, 0.03 g of iron (III) nitrate nonahydrate, 0.5 g of urea and 80 mL of H_2O were mixed in a beaker with the subsequent ultrasonic treatment for 0.5 h. Then the mixture was transferred into a stainless steel autoclave with PTFE lining (100 mL) and maintained at 120 °C for 24 h. After the autoclave was cooled to room temperature, the suspension was filtered and washed with abundant water, and then dried at 100 °C for 12 h. Finally, it was calcined in N_2 stream at 450 °C for 4 h with the heating rate of 2 °C/min. The obtained catalyst was denoted as Fe_2O_3/CNTs-CP. The Fe_2O_3 supported on TiO_2 was synthesized by an impregnation method with the iron content unchanged and denoted as Fe_2O_3/TiO_2.

2.2 Characterization

The morphologies and surface structure of the catalysts were observed by transmission electron microscope (TEM, JEOL JEM-200CX) and field emission high resolution transmission electron microscope (HRTEM, JEOL JEM-2100F). The energy dispersive X-ray spectroscopy (EDS) was carried out on a TEM (JEOL JEM-2100F). Powder X-ray diffraction (XRD) was performed with a Rigaku D/MAX-2200 X-ray diffractometer using Cu Kα (40 kV, 40 mA) radiation and a secondary beam graphite monochromater. Nitrogen adsorption-desorption isotherms of the samples were measured at 77 K using an ASAP 2020 volumetric adsorption analyzer. Before the measurements, all the samples were degassed overnight at 573 K in a vacuum line. The specific surface area and the pore volume of the samples were calculated by the Brunauer-Emmett-Teller (BET) method and the pore size distributions were derived from the adsorption branches of the isotherms using the Barrett-Joyner-Halenda (BJH) model. The Raman spectra were recorded on a spectrometer (JY H800UV) equipped with an optical microscope at room temperature. X-Ray photoelectron spectroscopy (XPS) was recorded on a Perkin-Elmer PHI-5000C ESCA system equipped with a dual X-ray source, using an Mg Kα (1253.6 eV) anode and a

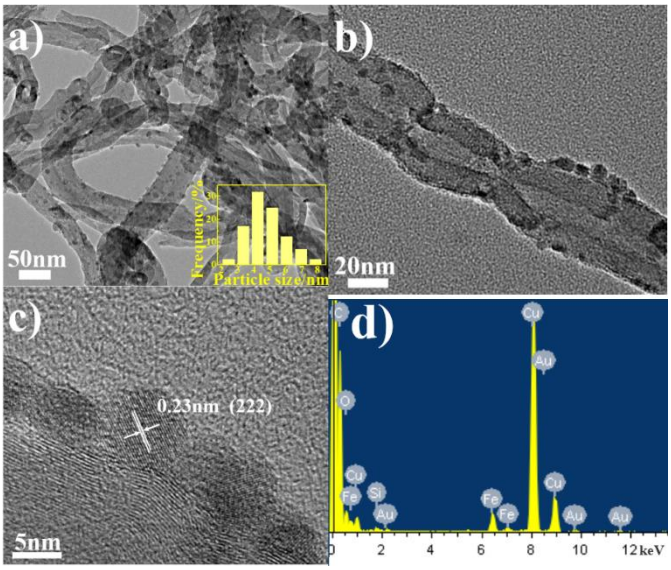

Fig. 1 (a, b) TEM images of Fe_2O_3/CNTs-ET; (c) HRTEM image of Fe_2O_3/CNTs-ET; (d) EDS spectrum of Fe_2O_3/CNTs-ET; size distribution of ferric oxide nanoparticles of Fe_2O_3/CNTs-ET (inlet).

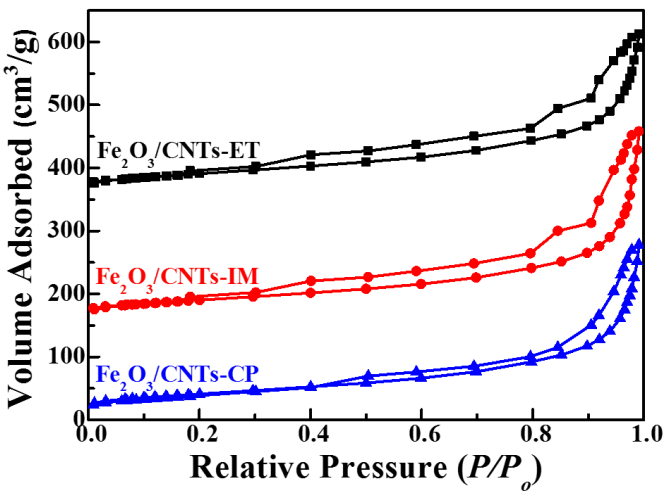

Fig. 2 N_2 adsorption-desorption isotherms of Fe_2O_3/CNTs-ET, Fe_2O_3/CNTs-IM and Fe_2O_3/CNTs-CP.

hemispherical energy analyzer. The background pressure during data acquisition was kept below 10^{-6} Pa. The XPS species of the elements in these catalysts were recorded and fitted by XPS PEAK 4.1 software, which had been calibrated against the standardized C 1s peak at 284.6 eV. Temperature-programmed reduction by hydrogen (H_2-TPR) was obtained on a Tianjin XQ tp5080 auto-adsorption apparatus. 50 mg of the catalyst was outgassed at 300 ^oC under N_2 atmosphere. After cooling to room temperature under N_2 atmosphere. The flowing gas was switched to 5 % H_2/N_2 and the sample was heated to 840 ^oC at a heating rate of 10 ^oC/min. The H_2 consumption was monitored by a thermal conductivity detector (TCD). Temperature-programmed desorption experiments of ammonia (NH_3-TPD) were conducted on a Tianjin XQ tp5080 auto-adsorption apparatus. Before the TPD, each sample was pretreated with high-purity (99.999 %) He (35 mL min^{-1}) at 300 ^oC for 0.5 h and then saturated with high-purity anhydrous ammonia at 100 ^oC for 1 h and subsequently flushed at the same temperature for 1 h to remove physical-adsorbed ammonium. Finally, the TPD operation was carried out from 100 ^oC to 525 ^oC at a heating rate of 10 ^oC/min. The amount of NH_3 desorbed was monitored by a TCD.

2.3 Catalytic tests

The NH_3-Selective Catalytic Reduction activity tests were completed in a fixed-bed quartz reactor by using 0.2 g catalyst (40-60 mesh). The mixture gases were composed of 500 ppm NO, 500 ppm NH_3, 3 vol.% O_2, the balance N_2, 200 ppm SO_2 (when used) and 4 vol.% H_2O (when used). The gas hourly space velocity (GHSV) was about 18, 000 h^{-1} with the total flow rate of the feed gas was approximately 220 mL min^{-1}. The reaction temperature was starting from 150 ^oC to 400 ^oC. All the concentration of the feed gas and the tail gases were detected by a KM9106 flue gas analyzer with the reaction reached 15 min.

3. Results & discussion

3.1 Characteristics of the catalysts

The microstructures of the catalysts and the size distribution of ferric oxide nanoparticles supported on the surface of CNTs were investigated by TEM. As shown in Fig. 1a and 1b, the TEM images of Fe_2O_3/CNTs-ET exhibited a homogeneously dispersion of ferric oxide nanoparticles supported on the surface of CNTs and the particle size is uniform. The HRTEM image in Fig. 1c shows the inter-planar distance is 0.23 nm, which is related to (222) plane of Fe_2O_3. Fig. 1d presents the EDS spectrum of Fe_2O_3/CNTs and confirms the presence of iron elements, which suggests the Fe species support on the surface of CNTs. As can be seen in Fig. 1 inlet, it was observed that the sizes of ferric oxides nanoparticles on the CNTs were in the range of 2.5-8.0 nm and the average size of nanoparticles was 4.8 nm. However, for Fe_2O_3/CNTs-IM, the particles aggregated to some extent (Fig. S1a, ESI); and for Fe_2O_3/CNTs-CP and Fe_2O_3/TiO_2, Fe_2O_3 nanoparticles display a distinct agglomeration (Fig. S1b and c, ESI). These indicate that the active components are uniformly anchored on the surface of CNTs by the ethanol-thermal method. Moreover, for Fe_2O_3/CNT-ET, the XRD peaks assigned to Fe_2O_3 were negligible, which suggested the good dispersion of Fe species (Fig. S2, ESI). It is confirmed that the Fe_2O_3 nanoparticles can be highly dispersed on CNTs by the ethanol-thermal method.

The specific surface area, pore volume and pore size of the catalysts were analyzed by N_2 adsorption-desorption isotherms. As displayed in Fig. 2, the Fe_2O_3 nanoparticles supported on CNTs by three different methods imply the IV isotherm with the relative pressure (P/P_o=0.15), indicating that the existence of mesoporous structure, and Fe_2O_3/TiO_2 also presents the mesoporous structure due to the stack of particles (Fig. S3, ESI). In addition, the specific surface area, pore volume and pore size

Table 1 BET surface area and pore characterization of catalysts.

	Fe_2O_3/CNTs-ET	Fe_2O_3/CNTs-IM	Fe_2O_3/CNTs-CP	Fe_2O_3/TiO_2
BET surface area (m^2/g)	147	144	146	55
Pore volume (cm^3/g)	0.41	0.48	0.43	0.33
Pore size (Å)	95	110	101	199

of the catalysts are summarized in Table 1. As shown directly in Table 1, there is no obvious difference among the three catalysts. Moreover, the BET surface area of Fe_2O_3/CNTs catalysts is about 145 m^2/g, which is higher than that of Fe_2O_3/TiO_2.

The Raman spectroscopy is a powerful tool in probing the lattice vibrational states and dynamics of CNTs, under the variation of the layer number in respect to the CNTs surface plane.[46-49] The Raman spectra of Fe_2O_3/CNTs prepared by three routes are displayed in Fig. 3. The G-band, which at around 1580 cm^{-1}, is associated with an E_{2g} mode of graphite and is related to the vibration of sp^2 bonded carbon atoms in a 2-dimensional hexagonal lattice. The D-band, which centred around 1360 cm^{-1}, is corresponding to the vibrations of carbon atoms with dangling bonds in plane terminations of disordered graphite or glassy carbon.[50-52] The I_D/I_G (the ratio of the intensities of the D and G bands) over Fe_2O_3/CNTs-ET, Fe_2O_3/CNTs-IM, Fe_2O_3/CNTs-CP and CNTs is around 1.02, 0.99, 0.89 and 0.81 (Fig. 3 and S4, ESI), respectively. Compared with the value of I_D/I_G over CNTs, Fe_2O_3/CNTs-ET are larger than the others, which suggest that more defects were created by introducing the active species.[52] Furthermore, the increased ratio of I_D/I_G indicates the increase of surface defects in the Fe_2O_3/CNTs-ET, [53] which should be favorable to the NH_3-SCR of NO. The Raman results of Fe_2O_3/CNTs and CNTs demonstrated that the structure of multi-wall CNTs can be retained after loaded with Fe_2O_3 nanoparticles.[50]

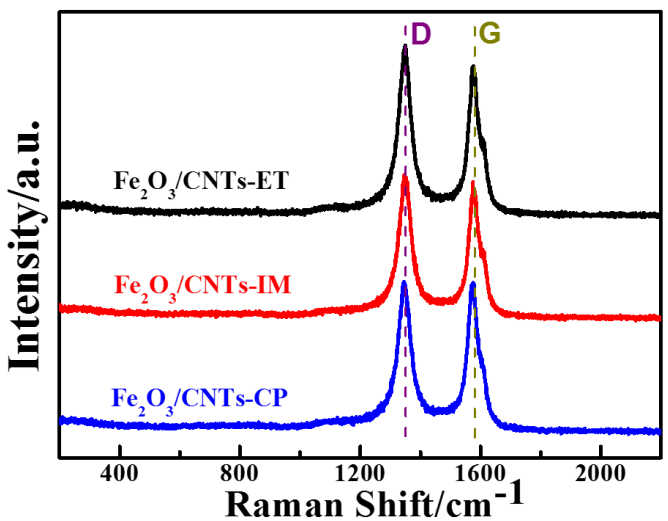

Fig. 3 Raman spectra of Fe_2O_3/CNTs-ET, Fe_2O_3/CNTs-IM and Fe_2O_3/CNTs-CP.

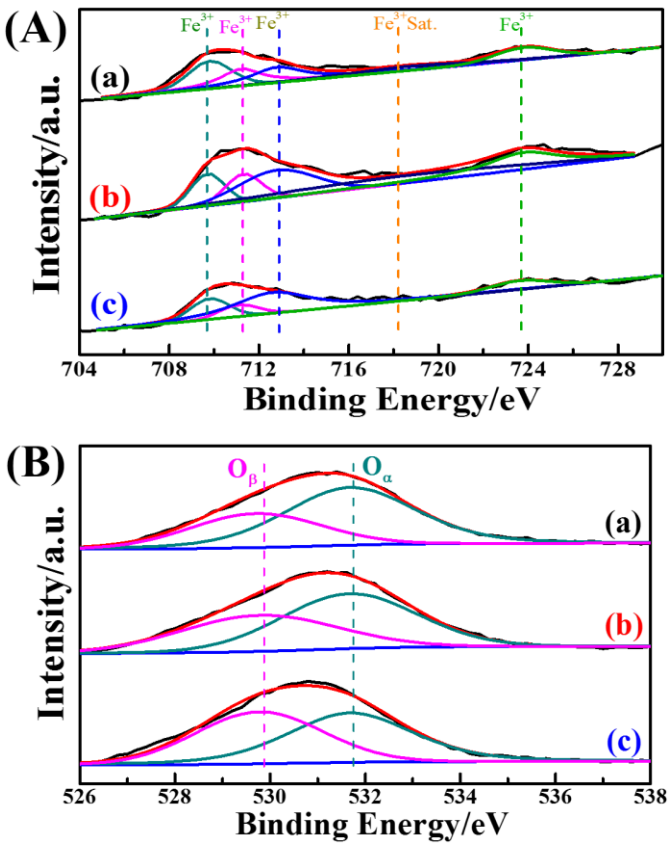

Fig. 4 (A) Fe 2p spectra and (B) O 1s spectra of the catalysts: (a) Fe_2O_3/CNTs-ET, (b) Fe_2O_3/CNTs-IM and (c) Fe_2O_3/CNTs-CP, respectively.

In order to acquire the information of the atomic concentrations and element chemical state of each catalyst's surface, the XPS spectra of the Fe 2p and O 1s in these catalysts were recorded. Fig. 4A shows the Fe peaks assigned to Fe species (Fe $2p_{3/2}$ and Fe $2p_{1/2}$). The Fe peaks of Fe_2O_3/CNTs were assigned to oxidized Fe species, more likely Fe^{3+} type species.[13, 54] The binding energies centered at about 709.8 eV and 711.2 eV may be assigned to Fe^{3+} in the spinel structure, and the binding energy centered at about 712.4 eV may be ascribed to Fe^{3+} bonded with hydroxyl group.[55] It is interesting that the surface atomic concentration of Fe over Fe_2O_3/CNTs-ET is higher than Fe_2O_3/CNTs-IM and Fe_2O_3/CNTs-CP as shown in Table 2. It has been demonstrated that the accessible Fe^{3+} can participate the reversible redox cycle which is beneficial for the SCR activity.[13] Based on the above results, it is reasonable that Fe_2O_3/CNTs-ET can display the best capacity for NH_3-SCR performance among the three catalysts.

The XPS spectra of O 1s of three catalysts are presented in Fig. 4B. All of three catalysts show two overlapping peaks of the O 1s. The overlapping peaks of O 1s at binding energy of 529.8 eV could be assigned to lattice oxygen (donated as O_β), and the overlapping peaks of O 1s at binding energies of about 531.7 eV could attributed to chemisorbed oxygen (donated as O_α), which could belong to defect oxide or hydroxyl-like groups.[27, 56-58] Table 2 summaries the binding energies of O 1s and the atomic ratio of $O_\alpha/(O_\alpha+O_\beta)$ of the three catalysts. As

Table 2 The Binding Energy and surface atomic concentration of catalysts.

Catalysts	Surface atomic concentration/%			Binding Energy/eV		The relative concentration ratios/%	
	C	Fe	O	O_β	O_α	$O_\beta/(O_\alpha+O_\beta)$	$O_\alpha/(O_\alpha+O_\beta)$
Fe_2O_3/CNTs-ET	92.93	0.43	7.64	529.8	531.7	34.45	65.55
Fe_2O_3/CNTs-IM	92.01	0.42	7.57	529.8	531.7	42.41	57.59
Fe_2O_3/CNTs-CP	92.19	0.23	7.59	529.8	531.7	47.81	52.19

seen clearly in Fig. 4B and Table 2, the Fe_2O_3/CNTs-ET owns a higher ratio of $O_\alpha/(O_\alpha+O_\beta)$ than the Fe_2O_3/CNTs-IM and Fe_2O_3/CNTs-CP, mainly on account of the increased chemisorbed oxygen species on the surface of catalyst by iron species.[27] The surface chemisorbed oxygen O_α has been reported to be the most active oxygen and highly active in the oxidation reaction due to its higher mobility. Besides, the high relative concentration ratio of $O_\alpha/(O_\alpha+O_\beta)$ on the surface of the catalyst could be correlated with the high NH_3-SCR activity.[59] The loading of Fe_2O_3 nanoparticles on CNTs by ethanol-thermal route could create more vacancies on the catalyst surface, and lead to the increase of chemisorbed oxygen on the surface. It is reported that the NO_2 would enhance the NH_3-SCR reaction with participating in the "fast SCR" reaction route on the catalysts.[15] It has been demonstrated that the chemisorbed oxygen plays an important role in oxidation reactions.[59] Therefore, the O_α plays a crucial role in NH_3-selective catalytic reduction process for promoting the oxidation of NO to NO_2.[60] Thus, the Fe_2O_3/CNTs-ET which possess the highest O_α content could be beneficial to improve the low-temperature NH_3-SCR catalytic activity, as expected.

The H_2-TPR measurements were extensively performed to investigate the reducibility of iron species in different catalysts. Fig. 5 presents the H_2-TPR profiles of different samples. In the

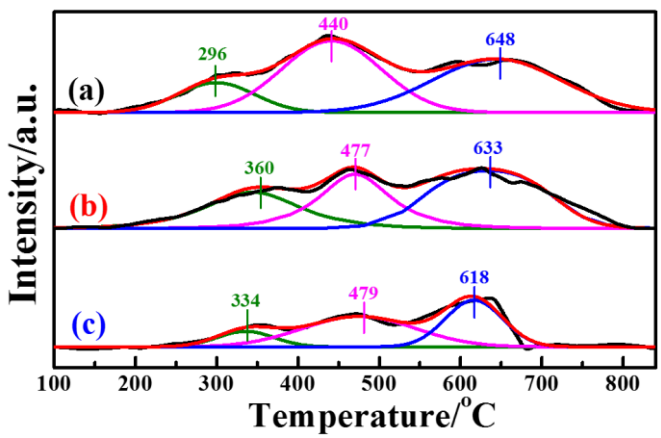

Fig. 5 H_2-TPR profiles of the catalysts: (a) Fe_2O_3/CNTs-ET, (b) Fe_2O_3/CNTs-IM and (c) Fe_2O_3/CNTs-CP.

Table 3 H_2 consumptions of catalysts.

	Catalysts		
	Fe_2O_3/CNTs-ET	Fe_2O_3/CNTs-IM	Fe_2O_3/CNTs-CP
Consumed hydrogen (mmol/g)	0.072	0.056	0.034

temperature scope of 100-840 °C, all of the three catalysts present three distinct H_2 consumption peaks, which were assigned to the three-stepwise reduction of $Fe_2O_3 \rightarrow Fe_3O_4$, $Fe_3O_4 \rightarrow FeO$, and $FeO \rightarrow Fe$.[25] For Fe_2O_3/TiO_2, the H_2-TPR profile showed the sequential reduction of Fe_2O_3 to Fe (Fig. S5a, ESI). Compared with Fe_2O_3/CNTs by each method, the corresponding reduction peaks of Fe_2O_3/CNTs-ET shifted to a relative low temperature. It should be pointed out that the area of the reduction peak has a direct relationship with the consumed content of H_2. It can be seen clearly that the area of the reduction peak over Fe_2O_3/CNTs-ET is the largest among the three catalysts. The H_2 consumption values of all the three Fe_2O_3/CNTs are given in Table 3. As shown in Table 3, Fe_2O_3/CNTs-ET gave the largest H_2 consumption among the three catalysts. In addition, the content of the reductive species related to the degree of dispersion, which suggest that Fe_2O_3 nanoparticles were highly dispersed on CNTs by the ethanol-thermal method. Thus, the Fe_2O_3/CNTs-ET can offer more active species, which can be in accordance with the results of the XPS results. Since more reductive species could enhance the NH_3-SCR reaction, the Fe_2O_3/CNTs synthesized by the ethanol-thermal route expose more reductive species which should be beneficial to the low-temperature NH_3-SCR performance.

The NH_3-TPD technique has been extensively used to characterize the adsorption of ammonia on the surface active sites of catalysts which acts a significant role in NH_3-SCR reaction. To investigate the surface acid amount and strength of the catalysts, the NH_3-TPD was performed. Fig. 6 shows the temperature-programmed desorption after ammonia adsorption over the three catalysts. It is clear that all of the three catalysts present three desorption peaks in the desorption temperature in the range of 100-525 °C. The peaks around 150-160 °C were caused by the desorption of weak acid sites; the peaks around 200-220 °C were caused by the medium acid sites; and the peaks around 390-420 °C were caused by the strong acid sites.[35] It is generally accepted that Lewis acid attributed to coordinated NH_3 molecules are thermally stable than Brønsted acid sites attributed to NH_4^+, so it can be inferred that the desorption peak at low temperature is assigned to physisorbed NH_3, and the desorption peak at high temperature is assigned to chemisorbed NH_3.[26, 59] It is demonstrated that the position and area of desorption peaks are correlated with the acid strength and acid amount, respectively.[41] The desorption peak of Fe_2O_3/CNTs by different methods locates at a relative same temperature, indicating that the acid site is similar among them.

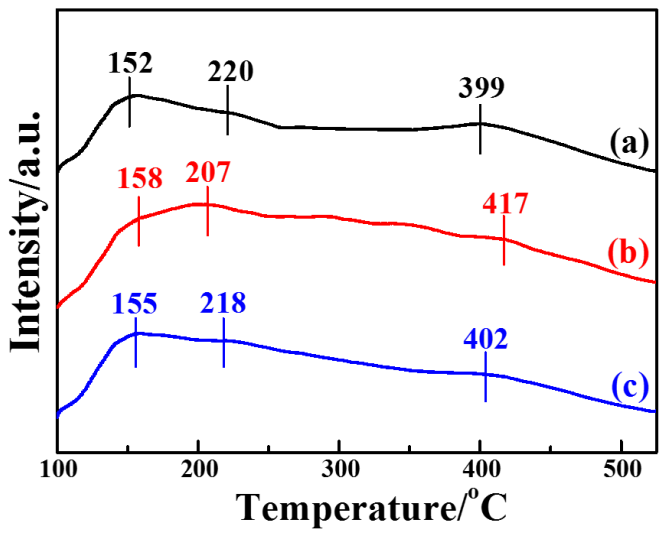

Fig. 6 NH_3-TPD profiles of the catalysts: (a) Fe_2O_3/CNTs-ET, (b) Fe_2O_3/CNTs-IM and (c) Fe_2O_3/CNTs-CP.

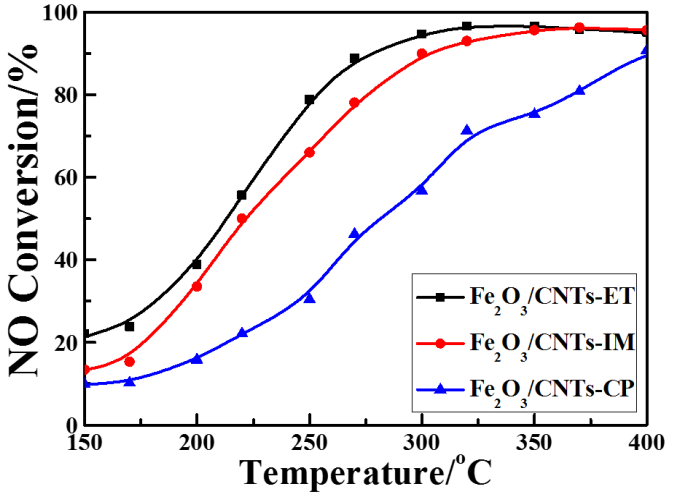

Fig. 7 NO conversion *vs.* temperature over the catalysts. *Reaction conditions:* [NO] = [NH_3] = 500ppm, [O_2] = 3 vol.%, N_2 balance, and GHSV= 18, 000 h^{-1}.

It is clear that the amount of adsorbed NH_3 of Fe_2O_3/CNTs-ET and Fe_2O_3/CNTs-IM is greater than that of Fe_2O_3/CNTs-CP. However, it is noteworthy that Fe_2O_3/CNTs-ET shows the higher Lewis acid sites than the other two Fe_2O_3/CNTs catalysts. For Fe_2O_3/TiO_2, the intensity of the desorption peaks adsorbed NH_3 is very weak and mainly concentrate at low temperature (Fig. S5b, ESI). It has been demonstrated that the CNTs themselves presented both weak acid sites and strong acid sites as a catalyst support.[28, 29] Besides, the results of NH_3-TPD imply that the synthesis route have a crucial effect on the amount of the acidic sites over the catalysts. As have been reported, the highly dispersed active species on the support could offer a large number of acidic sites and perform the best catalytic activity.[28] Therefore, the more amounts of the strongest acid sites over Fe_2O_3/CNTs-ET could be attributed to highly dispersed Fe_2O_3 nanoparticles and CNTs themselves.

3.2 Catalytic performance

Fig. 7 shows the NO conversion curves of the catalysts with reaction temperature ranging from 150 °C to 400 °C. It is clearly observed that the reaction temperature has a remarkable influence on the NO reduction efficiency over different catalysts. A negligible NO reduction efficiency was noticed for Fe_2O_3/CNTs-CP till the temperature reached 400 °C, whereas highly dispersed Fe_2O_3 nanoparticles on CNTs fabricated by the ethanol-thermal route displayed a favorable NH_3-SCR performance. The light-off temperature (at which the conversion of NO reaches 50 %, T_{50}) of Fe_2O_3/CNTs-ET is 220 °C, and the 96 % NO conversion is achieved at 320 °C. The Fe_2O_3/CNTs-ET shows the best low-temperature NO conversion among three catalysts and displays an excellent NH_3-SCR activity over a broad temperature window varying from 250 °C to 400 °C with the NO conversion higher than 80 %. It is noted that the Fe_2O_3/CNTs-ET also shows better performance at low temperature than Fe_2O_3/TiO_2 (Fig. S6, ESI). The difference of three catalysts could own to the different physical chemical characterizations of them. The results of TEM and XRD demonstrated that the Fe_2O_3 nanoparticles were uniformly anchored on the surface of CNTs over Fe_2O_3/CNTs-ET, which could be beneficial to the outstanding NH_3-SCR activity. Based on the results of Raman and XPS, for Fe_2O_3/CNTs-ET, it is clear that more defects Fe atoms exist on the catalyst surface, which indicates that more active sites are provided for SCR reaction. Besides, the highest content of chemisorbed oxygen would enhance the low-temperature NH_3-SCR reduction activity with accelerating the oxidation of NO to NO_2 during the "fast SCR" reaction. The results of the H_2-TPR indicated that the reducibility of Fe_2O_3/CNTs-ET was the strongest among the three catalysts, which could promote the NH_3-SCR reaction. Therefore, the robust reciprocities between ferric oxide and CNTs could cause the improvement of NH_3-SCR activity over Fe_2O_3/CNTs-ET.

The catalytic activity with time on stream is a significant item to estimate the catalysts' properties. Fig. 8A displays the catalytic activity of different catalysts with time on stream at 320 °C. All the catalysts are maintained unchanged and keep their highest conversion values during the whole test periods, and the Fe_2O_3/CNTs-ET shows the highest activity. It is noted that the oxidation of carbon nanotubes doesn't occur at this temperature during the SCR process, which has also been confirmed in our previous work [41, 61] As is well-known, there still exists some residual H_2O and SO_2 in the exhaust gas after the desulphurization process, which can poison and devitalize the catalysts in NH_3-SCR reaction.[3] Thus, it is worth noting that the NO conversion of the catalysts with the attendance of H_2O and SO_2. The influence of H_2O on the NH_3-SCR activity over the Fe_2O_3 supported on CNTs by three different methods as a function of time at 320 °C was investigated as shown in Fig. 8B. While introducing 4 vol.% H_2O to the feed gas, the NO conversion of all catalysts maintains unchanged during the whole test periods whether introducing H_2O or not. It is confirmed that the competitive adsorption between H_2O and NH_3 on the active sites of the catalyst surface could lead to the

Journal Name RSCPublishing

ARTICLE

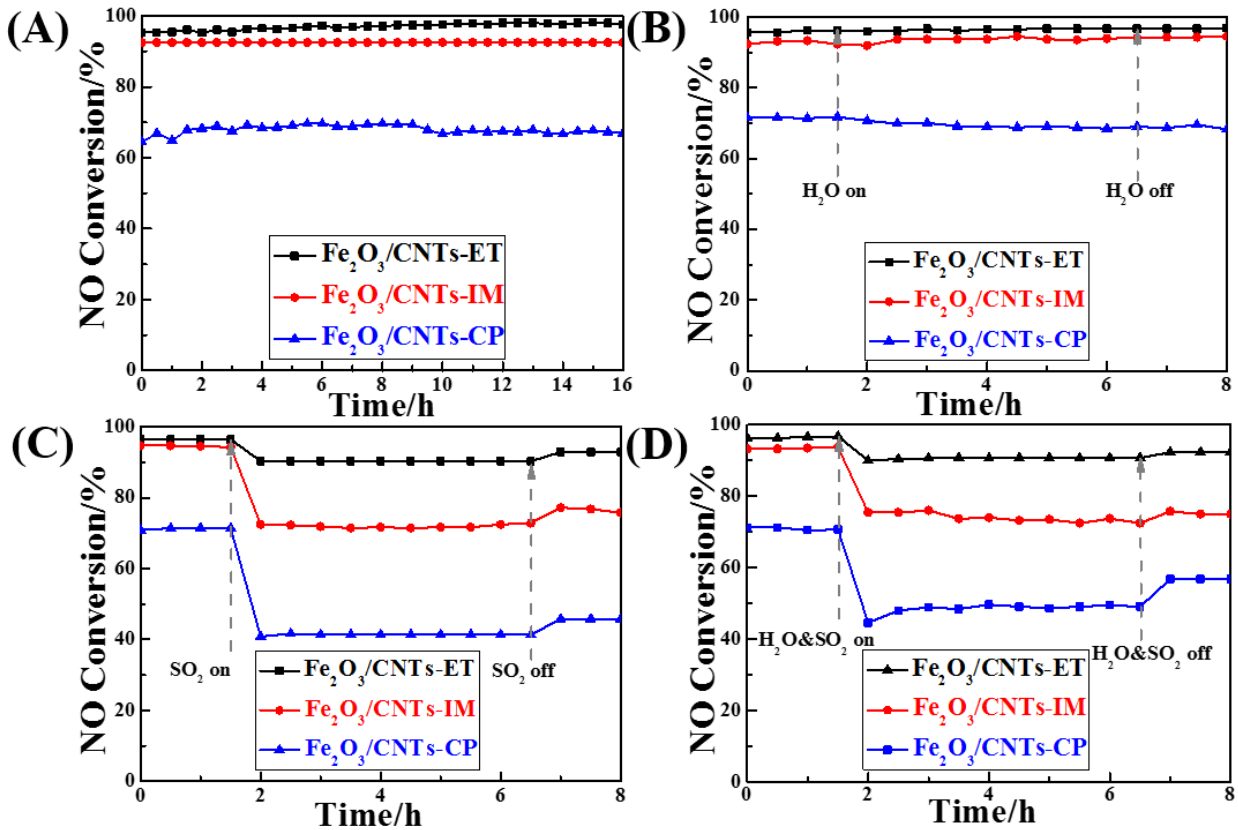

Fig. 8 (A) NO conversion *vs.* time on stream of the catalysts; (B) NO conversion *vs.* time on stream of the catalysts in the presence of H_2O; (C) NO conversion *vs.* time on stream of the catalysts in the presence of SO_2; (D) NO conversion *vs.* time on stream of the catalysts in the presence of H_2O and SO_2. *Reaction conditions:* [NO] = [NH_3] = 500 ppm, [O_2] = 3 vol.%, [SO_2] = 200 ppm (when used), [H_2O] = 4 vol.% (when used), N_2 balance, T = 320 °C and GHSV=18, 000 h^{-1}.

inhibition of H_2O. Combining with the NH_3-TPD results (Fig. 6), the Fe_2O_3/CNTs-ET could preferentially adsorb NH_3 other than H_2O in the feed gas, which shows a sum of the acid sites over Fe_2O_3/CNTs-ET, and then lead to an excellent H_2O resistance ability.[16] The above results suggested that the Fe_2O_3/CNTs-ET could be an appropriate candidate for H_2O resistance. Fig. 8C shows the results of SO_2 on the NO conversion of catalysts at the typical temperature of 320 °C. The total flow rate of the feed gas is 220 mL·min^{-1}. As shown in Fig. 8C, the NO conversion of Fe_2O_3/CNTs-ET is 97 % in the absence of SO_2, and decreases to 91 % while inletting SO_2 (200 ppm) in the feed gas. With persistently adding 200 ppm SO_2, the NO conversion of Fe_2O_3/CNTs-ET keeps stable. By contrast, the adding of SO_2 in the reaction condition induces a significant decrease of NO conversion over the Fe_2O_3/CNTs-IM and Fe_2O_3/CNTs-CP by 22 % and 30 %, respectively. After cutting off SO_2 from the feed gas, the conversion of NO of Fe_2O_3/CNTs-ET is restored to 92 % without any fluctuations during the test periods. However, for Fe_2O_3/CNTs-IM and Fe_2O_3/CNTs-CP, while eliminating the SO_2 stream the NO conversion of them is restored to a certain extent and finally returned to 77 % and 46 %, respectively. The above results indicate that the Fe_2O_3/CNTs-ET showed the best resistance to SO_2 among the three catalysts. It is well known that the SO_2 stream can poison and deactivate the catalyst with the formation and deposition of sulfates and bisulfates on the surface of the catalyst in NH_3-SCR reduction.[34, 35] At the same time, NH_3 is reacting with SO_2 instead of reacting with NO which could decrease the reaction between NH_3 and NO. Compared with the Fe_2O_3/CNTs-IM and Fe_2O_3/CNTs-CP, the Fe_2O_3/CNTs-ET presents a better resistance of SO_2. The results of NH_3-SCR activity under the reaction condition with the coexistence of H_2O and SO_2 over the catalysts were also investigated as shown in Fig. 8D. As can be seen clearly, the

activity of Fe_2O_3/CNTs-ET decrease only about 6 % after introducing 4 vol.% H_2O and 200 ppm SO_2 together, but the volume raised to 92 % while eliminating the mixture of H_2O and SO_2. By contrast, the NO conversions of Fe_2O_3/CNTs-IM and Fe_2O_3/CNTs-CP presented radically decrease by 18 % and 26 % under the mixture of 4 vol.% H_2O and 200 ppm SO_2, respectively; and then recovered to 75 % and 57 %, respectively after cutting off H_2O and SO_2. The above results shows that the Fe_2O_3/CNTs-ET possess a good capacity for the resistance of water and sulfur dioxide.

4. Conclusions

In summary, Fe_2O_3 nanoparticles anchored on CNTs were *in situ* prepared via an ethanol-thermal route for selective catalytic reduction of NO with NH_3. The Fe_2O_3/CNT-ET presented better NH_3-SCR performance, higher H_2O-resistance and SO_2 tolerance than the catalysts synthesized by impregnation or co-precipitation routes. Besides, it also presents a better NH_3-SCR activity compared with Fe_2O_3/TiO_2. The outstanding NH_3-SCR activity over Fe_2O_3/CNT-ET could be attributed to the high dispersion of Fe_2O_3 nanoparticles on CNTs, most defects of the surface, the robust reducibility and the larger amount of stronger acid strength and chemisorbed oxygen. According to the above excellent properties, the Fe_2O_3/CNT-ET catalyst might be a proper candidate for NH_3-SCR of NO with NH_3.

Acknowledgements

The authors acknowledge the support of the National Natural Science Foundation of China (51108258) and the Shanghai Municipal Education Commission (14ZZ097). We thank Prof. W. J. Yu and Prof. B. Lu from the Analysis and Test Centre of SHU for help with the TEM and Raman measurements. The authors would like to thank Dr. K. Zhang from the Analysis and Test Centre of NERCN for help with the HRTEM measurements.

Notes and references

Research Center of Nano Science and Technology, Shanghai University, Shanghai 200444, China. E-mail: dszhang@shu.edu.cn; Fax: +86 021 66136079; Tel: +86 021 66136081.

†Electronic Supplementary Information (ESI) available: TEM images of Fe_2O_3/CNTs-IM, Fe_2O_3/CNTs-CP, Fe_2O_3/TiO_2; XRD patterns of the samples; Nitrogen adsorption–desorption isotherm, H_2-TPR, NH_3-TPD profiles and NO conversion *vs.* temperature over the Fe_2O_3/TiO_2, and Raman spectrum of CNTs. See DOI: 10.1039/b000000x/

1. H. Bosch and F. Janssen., *Catal. Today*, 1988, **2**, 369-379.
2. W. C. Wang and N. D. Sze, *Nature*, 1980, **286**, 589-590.
3. J. M. Hao, H. Z. Tian and Y. Q. Lu, *Environ. Sci. Technol.*, 2002, **36**, 552-560.
4. P. Forzatti, I. Nova and E. Tronconi, *Angew. Chem. Int. Ed.*, 2009, **121**, 8516-8518.
5. P. G. Smirniotis, D. A. Pena and B. S. Uphade, *Angew. Chen. Int. Ed.*, 2001, **40**, 2479-2482.
6. P. G. W. A. Kompioa, A. Brückner, F. Hipler, G. Auer, E. Löffler and W. Grünert, *J. Catal.*, 2012, **286**, 237-247.
7. M. H. Groothaert, K. Lievens, H. Leeman, B. M. Weckhuysen and R. A. Schoonheydt, *J. Catal.*, 2003, **220**, 500-512.
8. P. J. Smeets, M. H. Groothaert, R. M. Teeffelen, H. Leeman, E. J.M. Hensen and R. A. Schoonheydt, *J. Catal.*, 2007, **245**, 358-368.
9. C. Shi, Y. Y. Ji, U. M. Graham, G. Jacobs, M. Crocker, Z. S. Zhang, Y. Wang and T. J. Toops, *Appl. Catal., B*, 2012, **119-120**, 183-196.
10. D. H. Lee, K. T. Kim, H. S. Kang, Y. H. Song and J. E. Park, *Environ. Sci. Technol.*, 2013, **47**, 10964-10970.
11. R. Q. Long and R. T. Yang, *J. Am. Chem. Soc.*, 1999, **121**, 5595-5596.
12. G. S. Qi and R. T. Yang, *Appl. Catal., B*, 2003, **44**, 217-225.
13. R. H. Gao, D. S. Zhang, X. G. Liu, L. Y. Shi, P. Maitarad, H. R. Li, J. P. Zhang and W. G. Cao, *Catal. Sci. Technol.*, 2013, **3**, 191-199.
14. H. L. Li, D. S. Zhang, P. Maitarad, L. Y. Shi, R. H. Gao, J. P. Zhang and W. G. Cao, *Chem. Commun.*, 2012, **48**, 10645-10647.
15. L. Zhang, L. Y. Shi, L. Huang, J. P. Zhang, R. H. Gao and D. S. Zhang, *ACS Catalysis*, 2014, **4**, 1753-1763.
16. X. L. Mou, B. S. Zhang, Y. Li, L. D. Yao, X. J. Wei, D. S. Su and W. J. Shen, *Angew. Chem. Int. Ed.*, 2012, **51**, 2989-2993.
17. R. Q. Long and R. T. Yang, *J. Catal.*, 1999, **188**, 332-339.
18. A. Z. Ma and W. Grunert, *Chem. Commun.*, 1999, 71-72.
19. G. S. Qi and R. T. Yang, *Catal. Lett.*, 2005, **100**, 243-246.
20. M. Schwidder, M. S. Kumar, K. Klementiev, M. M. Pohl, A. Bruckner and W. Grunert, *J. Catal.*, 2005, **231**, 314-330.
21. S. Brandenberger, O. Krocher, A. Tissler and R. Althoff, *Appl. Catal., B*, 2010, **95**, 348-357.
22. T. Zhang, J. Liu, D. X. Wang, Z. Zhao, Y. C. Wei, K. Cheng, G. Y. Jiang and A. J. Duan, *Appl. Catal., B*, 2014, **148-149**, 520-531.
23. P. Balle, B. Geiger and S. Kureti, *Appl. Catal., B*, 2009, **85**, 109-119.
24. P. Balle, B. Geiger, D. Klukowski, M. Pignatelli, S. Wohnrau, M. Menzel, I. Zirkwa, G. Brunklaus and S. Kureti, *Appl. Catal., B*, 2009, **91**, 587-595.
25. G. Neri, A. M. Visco, S. Galvagno, A. Dunato and M. Panzalorto, *Thermochim. Acta*, 1999, **329**, 39-46.
26. R. Q. Long and R. T. Yang, *J. Catal.*, 2002, **207**, 158-165.
27. Y. Shu, H. Sun, X. Quan and S. Chen, *J. Phys. Chem. C*, 2012, **116**, 25319-25327.
28. C. Fang, D. Zhang, L. Shi, R. Gao, H. Li, L. Ye and J. Zhang, *Catal. Sci. Technol.*, 2013, **3**, 803-811.
29. H. Chang, J. D. Lee, S. M. Lee and Y. H. Lee, *Appl. Phys. Lett.*, 2001, **79**, 3863-3865.
30. R. Q. Long and R. T. Yang, *Ind. Eng. Chem. Res.*, 2001, **40**, 4288-4291.
31. S. Santucci, S. Picozzi, F. D. Gregorio, L. Lozzi, C. Cantalini, L. Valentini, J. M. Kenny and B. Delley, *J. Chem. Phys.*, 2003, **119**, 10904-10910.
32. J. Z. Luo, L. Z. Gao, Y. L. Leung and C. T. Au, *Catal. Lett.*, 2000, **66**, 91–97.
33. Z. Zeng, P. Lu, C. T. Li, L. Mai, Z. Li and Y. S. Zhang, *Catal. Sci. Technol.*, 2012, **2**, 2188-2199.
34. S. L. Bai, J. H. Zhao, W. Li and Z. P. Zhu, *Catal. Today*, 2010, **158**, 393-400.
35. Z. X. Ma, H. S. Yang, Q. Li, J. W. Zheng and X. B. Zhang, *Appl. Catal., A*, 2012, **427-428**, 43-48.

36. B. C. Huang, R. Huang, D. J. Jin and D. Q. Ye, *Catal. Today*, 2007, **126**, 279-283.
37. J. Z. S. Bai, L. Wang and Z. Zhu, *J. Fuel Chem. and Technol.*, 2009, **37**, 583-587.
38. E. C. Vermisoglou, G. E. Romanos, G. N. Karanikolos and N. K. Kanellopoulos, *J. Hazard. Mater.*, 2011, **194**, 144-155.
39. X. Y. Fan, F. M. Qiu, H. S. Yang, W. Tian, T. F. Hou and X. B. Zhang, *Catal. Commun.*, 2011, **12**, 1298-1301.
40. S. Q. Song and S. J. Jiang, *Appl. Catal., B*, 2012, **117-118**, 346-350.
41. D. S. Zhang, L. Zhang, L. Y. Shi, C. Fang, H. R. Li, R. H. Gao, L. Huang and J. P. Zhang, *Nanoscale*, 2013, **5**, 1127-1136.
42. J. D. Xu, K. T. Zhu, X. F. Weng, W. Z. Weng, C. J. Huang and H. L. Wan, *Catal. Today*, 2013, **215**, 86-94.
43. Q. Li, H. S. Yang, F. M. Qiu and X. B. Zhang, *J. Hazard. Mater.*, 2011, **192**, 915-921.
44. Z. X. Ma, H. S. Yang, F. Liu and X. B. Zhang, *Appl. Catal., A*, 2013, **467**, 450-455.
45. D. S. Zhang, L. Zhang, L. Y. Shi, C. Fang, H. R. Li, R. H. Gao, L. Huang and J. P. Zhang, *RSC Adv.*, 2013, **3**, 8811-8819.
46. B. Tang, G. X. Hu and H. Y. Gao., *Appl. Spectrosc. Rev.*, 2010, **45**, 369-407.
47. L. M. Malard, M. A. Pimenta, G. Dresselhaus and M. S. Dresselhaus., *Phys. Rep.*, 2009, **473**, 51-87.
48. Y. F. Hao, Y. Y. Wang, L. Wang, Z. H. Ni, Z. Q. Wang, R. Wang, C. K. Koo, Z. X. Shen and J. T. L. Thong., *Small*, 2010, **6**, 195-200.
49. A. Gupta, G. Chen, P. Joshi, S. Tadigadapa and P. C. Eklund., *Nano Lett.*, 2006, **6**, 2667-2673.
50. X. J. Wang, J. Lu, Y. Xie, G. A. Du, Q. X. Guo and S. Y. Zhang, *J. Phys. Chem. B*, 2002, **106**, 933-937.
51. L. Zhang, Z. Jia, L. M. Huang, S. O'Brien and Z. H. Yu, *J. Phys. Chem. C*, 2007, **111**, 11240-11245.
52. M. S. Dresselhaus, G. Dresselhaus and A. Jorio, *J. Phys. Chem. C*, 2007, **111**, 17887-17893.
53. S. L. Chou, J. Z. Wang, Z. X. Chen, H. K. Liu and S. X. Dou, *Nanotechnology*, 2011, **22**, 265401.
54. T. Yamashita and P. Hayes, *Appl. Surf. Sci.*, 2008, **254**, 2441-2449.
55. S. J. Yang, C. Z. Wang, L. Ma, Y. Peng, Z. Qu, N. Q. Yan, J. H. Chen, H. Z. Chang and J. H. Li, *Catal. Sci. Technol.*, 2013, **3**, 161-168.
56. M. Kang, E. D. Park, J. M. Kim and J. E. Yie, *Appl. Catal., A*, 2007, **327**, 261-269.
57. P. Maitarad, D. S. Zhang, R. H. Gao, L. Y. Shi, H. R. Li, L. Huang, T. Rungrotmongkol and J. P. Zhang, *The Journal of Physical Chemistry C*, 2013, **117**, 9999-10006.
58. S. X. Cai, D. S. Zhang, L.Y. Shi, J. X., L. Zhang, L. Huang, H. R. Li and a. J. P. Zhang, *Nanoscale*, 2014, **6**, 7346-7353.
59. B. Guan, H. Lin, L. Zhu and Z. Huang, *J. Phys. Chem. C*, 2011, **115**, 12850-12863.
60. S. X. Cai, D. S. Zhang, L.Y. Shi, J. Xu, L. Zhang, L. Huang, H. R. Li and J. P. Zhang, *Catal. Sci. Technol.*, 2014, **4**, 93-101.
61. L. Zhang, D. S. Zhang, J. P. Zhang, S. X. Cai, C. Fang, L. Huang, H. R. Li, R. H. Gao and L. Y. Shi, *Nanoscale*, 2013, **5**, 9821-9829.